

**Electrochemical Supercapacitor Behavior of  
Nanoparticulate Rutile-type  $\text{Ru}_{1-x}\text{V}_x\text{O}_2$**

Katsunori Yokoshima, Takuyoshi Shibutani, Masashi Hirota, Wataru Sugimoto,\*  
Yasushi Murakami, Yoshio Takasu

Department of Fine Materials Engineering, Faculty of Textile Science and Technology,  
Shinshu University, 3-15-1 Tokida, Ueda 386-8567, JAPAN

Phone : +81-268-21-5455

Fax : +81-268-21-5452

E-mail : [wsugi@shinshu-u.ac.jp](mailto:wsugi@shinshu-u.ac.jp)

### Abstract

Rutile-type  $\text{Ru}_{1-x}\text{V}_x\text{O}_2$  nanoparticles possessing high surface area were prepared by a polymerizable-complex method and its electrochemical supercapacitor behavior was studied. X-ray diffractometry, energy-dispersive X-ray analysis, and  $\text{N}_2$  adsorption/desorption measurements were used to characterize the structure of the products. The electrochemical supercapacitor behavior of thick and thin films was studied by cyclic voltammetry in various acidic, neutral, and alkaline electrolytes.  $\text{Ru}_{1-x}\text{V}_x\text{O}_2$  exhibited extremely enhanced supercapacitive properties compared to pure  $\text{RuO}_2$ . The highest surface redox activity was achieved with an acidic electrolyte.  $\text{Ru}_{1-x}\text{V}_x\text{O}_2$  showed negligible surface redox activity in neutral electrolytes.

*Key Words:* Electrochemical capacitor; Supercapacitor; Rutile; Ruthenium Oxide; Cyclic Voltammetry

## 1. Introduction

Electrochemical supercapacitors have attracted increased interest due to their higher power density and longer cycle life compared to batteries, and higher energy density compared to conventional capacitors [1-5]. In particular, electrochemical supercapacitors based on metal oxides can generally provide higher energy density than conventional carbon materials, and better electrochemical stability than polymer materials [5-11].

Since the discovery of the outstanding capacitive characteristics of hydrous ruthenium oxide [12,13], many studies have centered on the increase in the utilization of the precious metal to overcome the lack of its abundance [14-21]. Recent studies have shown that crystalline oxides possessing rutile [22-24], perovskite [25], or pyrochlore [26,27] structures are also promising electrode materials for supercapacitors. Although the gravimetric capacitance of these anhydrous crystalline material are usually lower than hydrous ruthenium oxides, specific surface charge exceeding  $1000 \mu\text{C cm}^{-2}$  has been reported [13]. We previously reported that the specific charge of a  $\text{RuO}_2(33\%)\text{-VO}_2(67\%)/\text{Ti}$  electrode is about 50 times higher compared to a  $\text{RuO}_2/\text{Ti}$  electrode [22]. In a recent communication, we reported the supercapacitive behavior of rutile-type  $\text{Ru}_{1-x}\text{V}_x\text{O}_2$  nanoparticles ( $x = 0, 0.15$  and  $0.65$ ) possessing high surface area [23]. Gravimetric capacitance of  $570 \text{ F g}^{-1}$  based on the oxide ( $1,210 \text{ F g}^{-1}$  based on  $\text{RuO}_2$ ) and specific surface charge of  $432 \mu\text{C cm}^{-2}$  was achieved. Here we report the effect of carbon additives to the capacitive behavior of nanoparticulate  $\text{Ru}_{1-x}\text{V}_x\text{O}_2$  thick films as well as the pseudocapacitive behavior of thin films in various electrolytes.

## 2. Experimental

The preparation of the Ru-V binary oxide was conducted by a polymerizable-complex method [28-31]. A mixture of  $\text{RuCl}_3 \cdot n\text{H}_2\text{O}$ ,  $\text{VO}(\text{OC}_3\text{H}_7)_3$ , citric acid ( $(\text{HOOCCH}_2)_2\text{C}(\text{OH})(\text{COOH})$ ),  $\text{CH}_3\text{OH}$  and ethylene glycol ( $\text{HOCH}_2\text{CH}_2\text{OH}$ ) was

thoroughly mixed at 25°C for 2 h then 60°C for 12 h. (HOOCCH<sub>2</sub>)<sub>2</sub>C(OH)(COOH) acts as the complexing agent for stabilizing Ru and V against precipitation. After evaporating CH<sub>3</sub>OH by heating at 80°C for 6 h, the solution was heated at 130°C for 6 h to obtain a rigid resin. The resin was then pyrolyzed in air at 350°C for 8 h. Final calcination was conducted at 400°C for 30 min in air. The final product was obtained by treatment with copious amounts of 1 M H<sub>2</sub>SO<sub>4</sub> to completely dissolve excess V<sub>2</sub>O<sub>5</sub>. Calcination lower than 400°C resulted in poor electrochemical stability.

The cation ratio in the products was determined by energy-dispersive X-ray (EDX; Horiba EMAX-7000) analysis. The experimental uncertainty of the cation ratio given throughout the manuscript was determined to be approximately ±10 atomic%. X-ray diffraction (XRD; Rigaku RINT-2550 with monochromated CuK $\alpha$  radiation) analysis was used to characterize the crystal structure. The specific-surface area was determined from N<sub>2</sub> adsorption/desorption measurements conducted with a Micromeritics ASAP2010 instrument. The Brunauer-Emmett-Teller (BET) equation was used to characterize the overall surface area and Barret-Joyner-Hallender (BJH) equation was used to determine the surface area in the mesoporous region. The BET surface area was used for the calculation of the specific surface charge. Field-emission scanning-electron microscopy (FE-SEM; Hitachi S-5000) was utilized for observation of the morphology.

A beaker-type electrochemical cell was used for the electrochemical measurements. The cell was equipped with a working electrode, a platinum mesh counter electrode, and an Ag/AgCl reference electrode. Electrode potentials will be referred to the reversible hydrogen electrode (RHE) potential scale. A Luggin capillary faced the working electrode at a distance of 2 mm. For Ru<sub>1-x</sub>V<sub>x</sub>O<sub>2</sub> thick films, a 1 cm<sup>2</sup> Pt mesh was painted with the active material, typically 5.0 to 10.0 mg, mixed with 1 mass% PTFE as a binder, followed by heat treatment at 350°C for 1 h. For the Ru<sub>1-x</sub>V<sub>x</sub>O<sub>2</sub> thin films, a mirror polished Glassy Carbon rod (5 mm diameter surface) was

modified with 40  $\mu\text{g}$  of  $\text{Ru}_{1-x}\text{V}_x\text{O}_2$ . Cyclic voltammetry was carried out typically between 0.1 and 1.3 V vs. RHE at 25°C using 0.5M  $\text{H}_2\text{SO}_4$ , 0.5 M  $\text{Na}_2\text{SO}_4$ , 0.5 M  $\text{K}_2\text{SO}_4$ , 1 M  $\text{KCl}$ , 1 M  $\text{NaOH}$ , and 1 M  $\text{KOH}$  electrolytes.

### 3. Results and Discussion

The cation ratios of the products are summarized in Table 1. A considerable decrease from the nominal cation ratio was observed, which is attributed to the acid leaching of the by-product  $\text{V}_2\text{O}_5$ . Notice that not all of the vanadium was leached by the acid treatment, suggesting the presence of insoluble vanadium species in the products. Figure 1 shows the XRD patterns of the products after the acid treatment. The XRD peaks deviate from pure  $\text{RuO}_2$  for the vanadium containing products, which can be interpreted as the incorporation of  $\text{V}^{4+}$  into the rutile-type structure. The XRD patterns for the products with  $\text{V}/(\text{Ru}+\text{V}) = 0, 0.15, 0.59, 0.65$  were successfully indexed based on a single-phase rutile-type structure. A biphasic product, two rutile-type phases possessing different cell parameters, was obtained for the intermediate compositions ( $\text{V}/(\text{Ru}+\text{V}) = 0.37$  and  $0.46$ ). The lack of monophasic products for these compositions is probably due to inadequate reaction of the Ru and V precursors under the present conditions. The obtained cell parameters and cation ratios for the monophasic products matched the values of  $\text{Ru}_{1-x}\text{V}_x\text{O}_2$  obtained by a conventional solid-state reaction [32], indicating the formation of  $\text{Ru}_{1-x}\text{V}_x\text{O}_2$ .

Typical FE-SEM images of  $\text{RuO}_2$  and  $\text{Ru}_{0.35}\text{V}_{0.65}\text{O}_2$  are shown in Fig. 2. The primary particle size observed by FE-SEM for pure  $\text{RuO}_2$  was 10 nm, while that for  $\text{Ru}_{0.35}\text{V}_{0.65}\text{O}_2$  was slightly smaller, about 5 nm. The overall and mesoporous specific-surface areas,  $S_{\text{BET}}$  and  $S_{\text{BJH}}$ , of the products are summarized in Table 1. The products are mainly mesoporous, as can be seen from the difference between  $S_{\text{BET}}$  and  $S_{\text{BJH}}$ . The  $S_{\text{BET}}$  values increased with the increase in vanadium content. The higher  $S_{\text{BET}}$  values for the products with higher vanadium content are due to the slightly smaller

particle size, as observed by FE-SEM.

In the absence of citric acid as the complexing agent, a mixture of RuO<sub>2</sub> and Ru metal with  $S_{\text{BET}} = 20 \text{ m}^2 \text{ g}^{-1}$  was obtained. Due to the low specific-surface area, the gravimetric capacitance was only  $7 \text{ F g}^{-1}$ . The addition of citric acid (polymerizable-complex method) resulted in RuO<sub>2</sub> with  $S_{\text{BET}} = 52 \text{ m}^2 \text{ g}^{-1}$  and gravimetric capacitance of  $70 \text{ F g}^{-1}$ . The addition of citric acid clearly affords a homogeneous product.

Cyclic voltammograms of Ru<sub>1-x</sub>V<sub>x</sub>O<sub>2</sub> thick films prepared by the polymerizable-complex method are shown in Fig. 3. The shape of the cyclic voltammograms was similar to those previously reported for DSA-type Ru-V-O/Ti electrodes [22]. The gravimetric capacitance is summarized in Table 1. As summarized in Table 1, the  $S_{\text{BET}}$  value for Ru<sub>0.35</sub>V<sub>0.65</sub>O<sub>2</sub> was about three times higher than that of RuO<sub>2</sub>. Hence, one reason for the high gravimetric capacitance of Ru<sub>0.35</sub>V<sub>0.65</sub>O<sub>2</sub> can be attributed to the increase in  $S_{\text{BET}}$ . If one assumes that the increase in  $S_{\text{BET}}$  is the sole cause for the increase in the gravimetric capacitance, the specific surface charge, which is a measure of the surface activity of the material, would remain constant. This is not the case for Ru<sub>1-x</sub>V<sub>x</sub>O<sub>2</sub>; the specific surface charge increased with the increase in the vanadium content from  $162 \mu\text{C cm}^{-2}$  for RuO<sub>2</sub> to  $450 \mu\text{C cm}^{-2}$  for Ru<sub>0.41</sub>V<sub>0.59</sub>O<sub>2</sub> (Table 1).

The cyclic voltammograms (Fig. 3) for Ru<sub>1-x</sub>V<sub>x</sub>O<sub>2</sub> indicates that the *i*-*E* response tends to deteriorate with the increase in the vanadium content. This is more clearly seen at higher scan rates, as shown in Fig. 4. The gravimetric capacitance for Ru<sub>0.35</sub>V<sub>0.65</sub>O<sub>2</sub> was  $190 \text{ F (g-oxide)}^{-1}$  at a scan rate of  $50 \text{ mV s}^{-1}$ . The capacitance retention ratio  $C/C_0$ , defined as the capacitance at  $\nu=50 \text{ mVs}^{-1}$  normalized to the capacitance at  $\nu=2 \text{ mVs}^{-1}$ , for Ru<sub>0.35</sub>V<sub>0.65</sub>O<sub>2</sub> is  $C/C_0 \sim 30\%$ , which is poor compared to pristine RuO<sub>2</sub> ( $C/C_0 \sim 60\%$ ). The  $C/C_0$  value was improved to 65% by physically mixing acetylene black (AB), as shown in Fig. 5. The intra-particle resistance, *i.e.*, the intrinsic

resistivity originating from the bulk resistivity of  $\text{Ru}_{1-x}\text{V}_x\text{O}_2$  of the present electrode material, should not decrease much compared to pure  $\text{RuO}_2$  because rutile-type  $\text{VO}_2$  possess metallic properties with resistivity of  $\sim 10^{-4} \Omega \text{ cm}$  [33], only one order higher than the room-temperature resistivity of  $\text{RuO}_2$  ( $\sim 10^{-5} \Omega \text{ cm}$ ) [34]. The resistivity of the carbon additive is higher, typically around  $\sim 10^{-1} \Omega \text{ cm}$ . Thus, neither the inter-particle nor the intra-particle contact resistance can explain the loss of specific capacitance at high scan rate. The addition of AB most likely provides extra mesopores for quick charge storage [16]. The capacitance decay for  $\text{Ru}_{0.35}\text{V}_{0.65}\text{O}_2$  mixed with 20 mass% AB at a scan rate of  $50 \text{ mV s}^{-1}$  was less than 5% after 10,000 cycles (Fig. 6).

Normalization of the capacitance by the amount of  $\text{RuO}_2$  present in the active material,  $C_{\text{RuO}_2}$ , allows an evaluation of the economic efficiency of the electrode material, in other words, the utilizability of the precious metal used in the products. A  $C_{\text{RuO}_2}$  value of  $1,210 \text{ F (g-RuO}_2\text{)}^{-1}$  ( $1,590 \text{ F (g-Ru)}^{-1}$ ) was obtained for  $\text{Ru}_{0.36}\text{V}_{0.64}\text{O}_2$  (Table 1), which exceeds that of  $\text{RuO}_2 \cdot n\text{H}_2\text{O}$  ( $760 \text{ F (g-material)}^{-1}$ ,  $1,200 \text{ F (g-Ru)}^{-1}$ ) [12,13]. The calculated  $C_{\text{RuO}_2}$  value is obviously an over-estimation since contribution of vanadium to the gravimetric capacitance most likely occurs. However, this value is important for understanding the cost performance of the electrode material.

In order to elucidate the redox contribution to the pseudocapacitive behavior, cyclic voltammetry was conducted in various electrolytes using thin film electrodes. Figure 7 shows cyclic voltammograms of  $\text{Ru}_{0.28}\text{V}_{0.72}\text{O}_2$  in acidic, neutral, and alkaline electrolytes at various scan rates. In the case of  $0.5 \text{ M H}_2\text{SO}_4$ , two redox couples are observed at 0.4 and 0.8 V. The gravimetric capacitance at a scan rate of  $2 \text{ mV s}^{-1}$  was  $C_{\text{oxide}} = 307 \text{ F (g-oxide)}^{-1}$  and  $C_{\text{RuO}_2} = 807 \text{ F (g-RuO}_2\text{)}^{-1}$ . The redox couples observed in  $0.5 \text{ M H}_2\text{SO}_4$  are not evident in neutral electrolytes. The scan rate independent current (1.3→0.6 V and 0.1→0.8 V) can be assumed as the electric double-layer charging. The electrochemically active surface area was about  $100 \text{ m}^2 \text{ g}^{-1}$  calculated from these

currents using the probe value [35] of  $C_{dl} = 80 \mu\text{F cm}^{-2}$  for the electric double-layer capacitance. In the case of nanoparticulate  $\text{RuO}_2$ , the total capacitance was deconvoluted into the electric double-layer capacitance, adsorption capacitance, and irreversible capacitance [35]. Although it is difficult to separate the total capacitance of  $\text{Ru}_{1-x}\text{V}_x\text{O}_2$  into 3 major reactions from the cyclic voltammograms in this study, the total surface charge ( $Q_{all}$ ) can be deconvoluted into the electric double-layer charge ( $Q_{dl}$ ) and the redox related charge ( $Q_{redox}$ ). The total surface charge for  $\text{Ru}_{0.28}\text{V}_{0.72}\text{O}_2$  in 0.5 M  $\text{H}_2\text{SO}_4$  was  $370 \mu\text{C cm}^{-2}$ . The redox related charge ( $Q_{redox}$ ) is thus  $274 \mu\text{C cm}^{-2}$  by subtraction of the electric double-layer capacitance ( $80 \mu\text{F cm}^{-2}$ ) [35]. The contribution of redox related charge ( $Q_{redox}$ ) to total surface charge ( $Q_{all}$ ) was 74%. In the case of  $\text{RuO}_2$ , the redox capacitance at a scan rate of  $2 \text{ mV s}^{-1}$  is only  $66 \mu\text{C cm}^{-2}$  (Table 1). Thus, the redox capacitance was tripled by the addition of vanadium.

In alkaline electrolytes (1 M NaOH and 1 M KOH), one redox couple is observed at  $\sim 0.6 \text{ V}$ . Since such redox activity is not observed for pure  $\text{RuO}_2$ , the redox couple can be attributed to the contribution from vanadium species. The gravimetric capacitance at a scan rate of  $2 \text{ mV s}^{-1}$  was  $C_{oxide} = 283 \text{ F (g-oxide)}^{-1}$  ( $C_{\text{RuO}_2} = 740 \text{ F (g-RuO}_2\text{)}^{-1}$ ) in NaOH and  $C_{oxide} = 271 \text{ F g}^{-1}$  ( $C_{\text{RuO}_2} = 705 \text{ F (g-RuO}_2\text{)}^{-1}$ ) in KOH. The redox related charge is thus  $Q_{redox} = 203 \mu\text{C cm}^{-2}$  in NaOH and  $Q_{redox} = 191 \mu\text{C cm}^{-2}$  in KOH. The contribution of redox related charge ( $Q_{redox}$ ) to total surface charge ( $Q_{all}$ ) was 72% in NaOH and 70% in KOH. The contribution of vanadium in alkaline electrolyte was slightly smaller than the case of 0.5 M  $\text{H}_2\text{SO}_4$ .

#### 4. Conclusion

A solid-solution  $\text{Ru}_{1-x}\text{V}_x\text{O}_2$  possessing a rutile-type structure was prepared by a polymerizable-complex method and its electrochemical supercapacitor behavior was

studied. Gravimetric capacitance of  $574 \text{ F (g-oxide)}^{-1}$ , or  $1,210 \text{ F (g-RuO}_2\text{)}^{-1}$ , was achieved for  $\text{Ru}_{0.35}\text{V}_{0.65}\text{O}_2$ . Evaluation of the specific surface charge of  $\text{Ru}_{1-x}\text{V}_x\text{O}_2$  indicated that the surface utilization was drastically increased by the increase in vanadium content. The addition of acetylene black to the electrode material improved the high-scan rate characteristics. In neutral electrolytes, most of the gravimetric capacitance was attributable to electric double-layer charging. The redox related charge in  $0.5 \text{ M H}_2\text{SO}_4$  was slightly larger than that in  $1 \text{ M NaOH}$  and  $1 \text{ M KOH}$ .

### **Acknowledgement**

This work was supported in part by an Industrial Technology Research Grant Program (02B63013c) from the New Energy and Industrial Technology Development Organization (NEDO) and Grants-in-Aid for Scientific Research (16750170, 17350097) and a 21st Century COE Program from Ministry of Education, Science, Sports, and Culture (MEXT).

## References

- [1] B.E. Conway, *Electrochemical Supercapacitors*, Kluwer Academic Pub., Norwell, MA, 1999.
- [2] I.E. Raistrick, in “*Electrochemistry of Semiconductors and Electronics*”, J. McHardy and F. Ludwig Editors, p.297, Noyes Publications, N.J. (1992).
- [3] A. Nishino, *J. Power Sources*, **60** (1996) 137-147.
- [4] E. Faggioli, P. Rena, V. Danel, X. Andriu, R. Mallant, H. Kahlen, *J. Power Sources*, **84** (1999) 261-269.
- [5] A. Burke, *J. Power Sources*, **91** (2000) 37-50.
- [6] B.E. Conway, *J. Electrochem. Soc.*, **138** (1991) 1539-1548.
- [7] S. Trasatti, *Electrochim. Acta*, **36** (1991) 225-241.
- [8] S. Sarangapani, B.V. Tilak, C.-P. Chen, *J. Electrochem. Soc.*, **143** (1996) 3791-3799.
- [9] B.E. Conway, V. Birss, J. Wojtowicz, *J. Power Sources*, **66** (1997) 1-14.
- [10] Y. Takasu, Y. Murakami, *Electrochim. Acta*, **45** (2000) 4135-4141.
- [11] C. Angelinetta, S. Trasatti, L.D. Atanasoska, R.T. Atanasoski, *J. Electroanal. Chem.*, **214** (1986) 535-546.
- [12] J.P. Zheng, T.R. Jow, *J. Electrochem. Soc.*, **142** (1995) L6-L8.
- [13] J.P. Zheng, P.J. Cyang, T.R. Jow, *J. Electrochem. Soc.*, **142** (1995) 2699-2703.
- [14] J.P. Zheng, T.R. Jow, *J. Power Sources*, **62** (1996) 155-159.
- [15] T.R. Jow, J.P. Zheng, *J. Electrochem. Soc.*, **145** (1998) 49-52.
- [16] J.P. Zheng, *Electrochem. Solid-State Lett.*, **2** (1999) 359-361.
- [17] Q.L. Fang, D.A. Evans, S.L. Roberson, J.P. Zheng, *J. Electrochem. Soc.*, **148** (2001) A833-A837.
- [18] Y.U. Jeong, A. Manthiram, *Electrochem. Solid-State Lett.*, **3** (2000) 205-208.
- [19] Y.U. Jeong, A. Manthiram, *J. Electrochem. Soc.*, **148** (2001) A189-A193.
- [20] C.-C. Hu, K.-H. Chang, *Electrochim. Acta*, **45** (2000) 2685-2696.

- [21] C.-C. Hu, Y.-H. Huang, *Electrochim. Acta*, **46** (2001) 3431-3444.
- [22] Y. Takasu, T. Nakamura, H. Ohkawauchi, Y. Murakami, *J. Electrochem. Soc.*, **144** (1997) 2601-2606.
- [23] W. Sugimoto, T. Shibutani, Y. Murakami, Y. Takasu, *Electrochem. Solid-State Lett.*, **5** (2002) A170-A172.
- [24] K. Yokoshima, W. Sugimoto, Y. Murakami, Y. Takasu, *Electrochem.*, **73**, (2005) 1026-1029.
- [25] P.M. Wilde, T.J. Guther, R. Oesten, J. Garche, *J. Electroanal. Chem.*, **461** (1999) 154-160.
- [26] H.J. Bang, W. Lu, F. Cao, J. Prakash, *Electrochem. Commun.*, **2** (2000) 653-657.
- [27] F. Cao, J. Prakash, *J. Power Sources*, **92** (2001) 40-44.
- [28] M.P. Pechini, U.S. Patent No. 3,330 (1967) 697.
- [29] M. Kakihana, L. Börjesson, S. Eriksson, P. Svedlindh, *J. Appl. Phys.*, **69** (1991) 867-873.
- [30] M. Kakihana, *J. Sol-Gel Sci. Technol.*, **5** (1996) 7-55.
- [31] M. Kakihana, M. Yoshimura, *Bull. Chem. Soc. Jpn*, **72** (1999) 1427-1443.
- [32] Y.S. Shorikov, M.B. Varfolomeev, E.A. Korablina, G.F. Khudorozhko, I.P. Asanov, *Russ. J. Inorg. Chem.*, **30** (1985) 934.
- [33] N.F. Mott, *Metal-Insulator Transitions*, Taylor & Francis Ltd (1974) , p.189.
- [34] W.D. Ryden, A.W. Lawson, C.C. Sartin, *Phys. Rev. B*, **1** (1969) 1494-1500.
- [35] W. Sugimoto, T. Kizaki, K. Yokoshima, Y. Murakami, Y. Takasu, *Electrochim. Acta*, **49** (2004) 313-320.

**Figure captions**

Fig.1. XRD patterns of the products with different V content of  $V/(Ru+V) =$  (a) 0, (b) 0.18, (c) 0.37, (d) 0.46, (e) 0.59, and (f) 0.65.

Fig.2. FE-SEM images of (a)  $RuO_2$  and (b)  $Ru_{0.35}V_{0.65}O_2$ .

Fig.3. Steady-state cyclic voltammograms of (a)  $RuO_2$ , (b)  $Ru_{0.82}V_{0.18}O_2$ , (c)  $Ru_{0.63}V_{0.37}O_2$ , (d)  $Ru_{0.54}V_{0.46}O_2$ , (e)  $Ru_{0.41}V_{0.59}O_2$ , and (f)  $Ru_{0.35}V_{0.65}O_2$  thick films in 0.5 M  $H_2SO_4$  at a scan rate of  $2\text{ mV s}^{-1}$ .

Fig.4. Steady-state cyclic voltammograms of (a)  $RuO_2$ , (b)  $Ru_{0.82}V_{0.18}O_2$ , (c)  $Ru_{0.63}V_{0.37}O_2$ , (d)  $Ru_{0.54}V_{0.46}O_2$ , (e)  $Ru_{0.41}V_{0.59}O_2$ , and (f)  $Ru_{0.35}V_{0.65}O_2$  thick films in 0.5 M  $H_2SO_4$  at a scan rate of  $50\text{ mV s}^{-1}$ .

Fig.5. Scan-rate dependence of the gravimetric capacitance for (a)  $RuO_2$ , (b)  $Ru_{0.82}V_{0.18}O_2$ , (c)  $Ru_{0.63}V_{0.37}O_2$ , (d)  $Ru_{0.54}V_{0.46}O_2$ , (e)  $Ru_{0.41}V_{0.59}O_2$ , (f)  $Ru_{0.35}V_{0.65}O_2$  thick films. (f') Scan-rate dependence of the gravimetric capacitance of a  $Ru_{0.35}V_{0.65}O_2$  thick film mixed with 20 mass% AB. The gravimetric capacitances were calculated from cyclic voltammograms between 0.1 and 1.3 V vs. RHE.

Fig. 6. Cyclability of  $Ru_{0.35}V_{0.65}O_2$  mixed with 20 mass% AB thick film at a scan rate of  $50\text{ mV s}^{-1}$  in 0.5 M  $H_2SO_4$ . The gravimetric capacitances were calculated from cyclic voltammograms at a scan rate of  $50\text{ mV s}^{-1}$  between 0.1 and 1.3 V vs. RHE.

Fig. 7 Cyclic voltammograms showing the differential capacitance of  $Ru_{0.28}V_{0.72}O_2$  thin films at scan rate of 500, 200, 50, 20, 5, and  $2\text{ mV s}^{-1}$  in various electrolytes.

Table I. Summary of the properties of the Ru<sub>1-x</sub>V<sub>x</sub>O<sub>2</sub> nanoparticles

V content, V/(Ru+V)		surface area / m <sup>2</sup> g <sup>-1</sup>		particle size / nm		lattice parameter / nm		Specific capacitance <sup>b)</sup>		
nominal	observed	S <sub>BET</sub>	S <sub>BJH</sub>	from BET	from XRD	<i>a</i>	<i>c</i>	C <sub>oxide</sub> / F g <sup>-1</sup>	C <sub>RuO<sub>2</sub></sub> / F g <sup>-1</sup>	Q <sub>BET</sub> / μC cm <sup>-2</sup>
0	0	52	58	16	9	0.4493(6)	0.3101(8)	70	70	162
0.50	0.18	83	77	11	6	0.4518(9)	0.304(2)	180	200	257
0.75 <sup>a)</sup>	0.37	105	95	9	N.D.	[0.458(6)] [0.450(6)]	[0.287(4)] [0.305(5)]	302	412	345
0.80 <sup>a)</sup>	0.46	124	74	8	N.D.	[0.459(5)] [0.450(5)]	[0.284(3)] [0.302(5)]	456	699	442
0.85	0.59	127	87	8	8	0.4599(9)	0.2853(7)	476	903	450
0.90	0.65	160	130	7	10	0.4605(7)	0.2840(6)	570	1,210	432

a) Biphasic products. Lattice parameters for both phases are shown. Particle size from XRD were not determined for biphasic products.

b) Calculated from cyclic voltammogram between 0.1 and 1.3 V at a scan rate of 2 mV s<sup>-1</sup>.

S<sub>BET</sub>; overall surface area determined by the BET equation

S<sub>BJH</sub>; mesoporous surface area determined by the BJH equation

C<sub>oxide</sub>; gravimetric capacitance per unit oxide mass

C<sub>RuO<sub>2</sub></sub>; gravimetric capacitance per unit RuO<sub>2</sub> mass

Q<sub>BET</sub>; specific charge per unit BET surface area

Table 2. Gravimetric capacitance of  $\text{Ru}_{0.28}\text{V}_{0.72}\text{O}_2$  in various electrolytes.

Scan rate / $\text{mV s}^{-1}$	Gravimetric capacitance / $\text{F (g-oxide)}^{-1}$					
	$\text{H}_2\text{SO}_4$	$\text{Na}_2\text{SO}_4$	$\text{K}_2\text{SO}_4$	KCl	NaOH	KOH
500	112	81	80	75	97	82
200	150	96	88	85	127	99
50	208	125	110	105	190	142
20	241	146	122	121	217	180
5	285	186	150	155	253	236
2	307	216	173	180	283	271

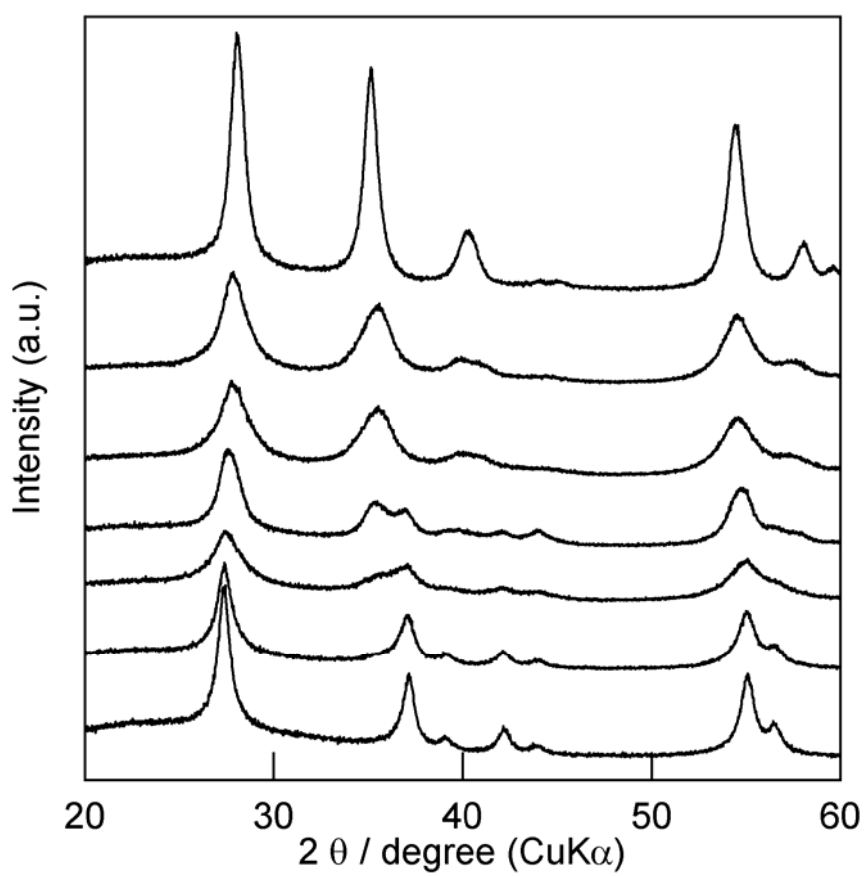


Fig.1. XRD patterns of the products with different V content of  $\text{V}/(\text{Ru}+\text{V}) =$  (a) 0, (b) 0.18, (c) 0.37, (d) 0.46, (e) 0.59, and (f) 0.65.

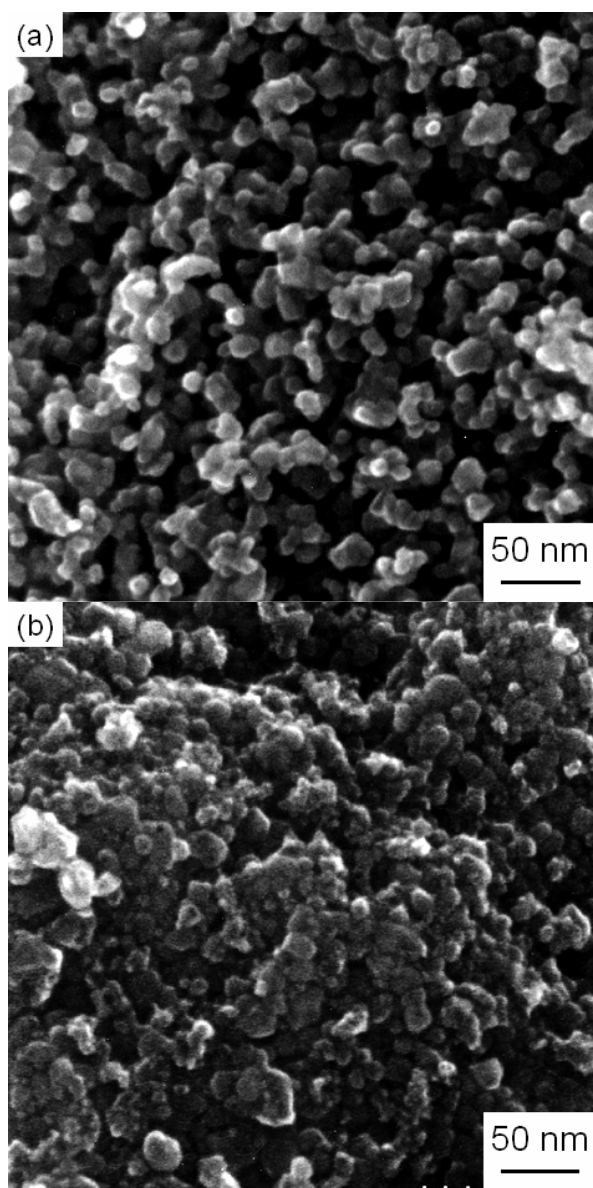


Fig.2. FE-SEM images of (a) RuO<sub>2</sub> and (b) Ru<sub>0.35</sub>V<sub>0.65</sub>O<sub>2</sub>.

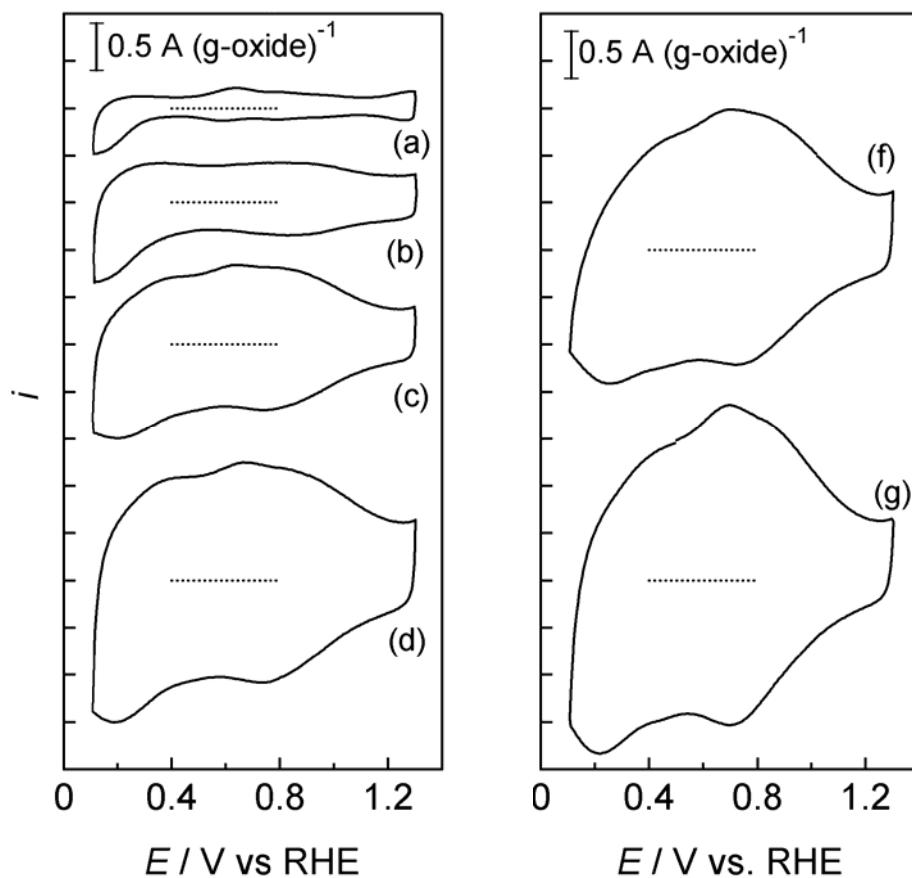


Fig.3. Steady-state cyclic voltammograms of (a)  $RuO_2$ , (b)  $Ru_{0.82}V_{0.18}O_2$ , (c)  $Ru_{0.63}V_{0.37}O_2$ , (d)  $Ru_{0.54}V_{0.46}O_2$ , (e)  $Ru_{0.41}V_{0.59}O_2$ , and (f)  $Ru_{0.35}V_{0.65}O_2$  thick films in 0.5 M  $H_2SO_4$  at a scan rate of  $2 mV s^{-1}$ .

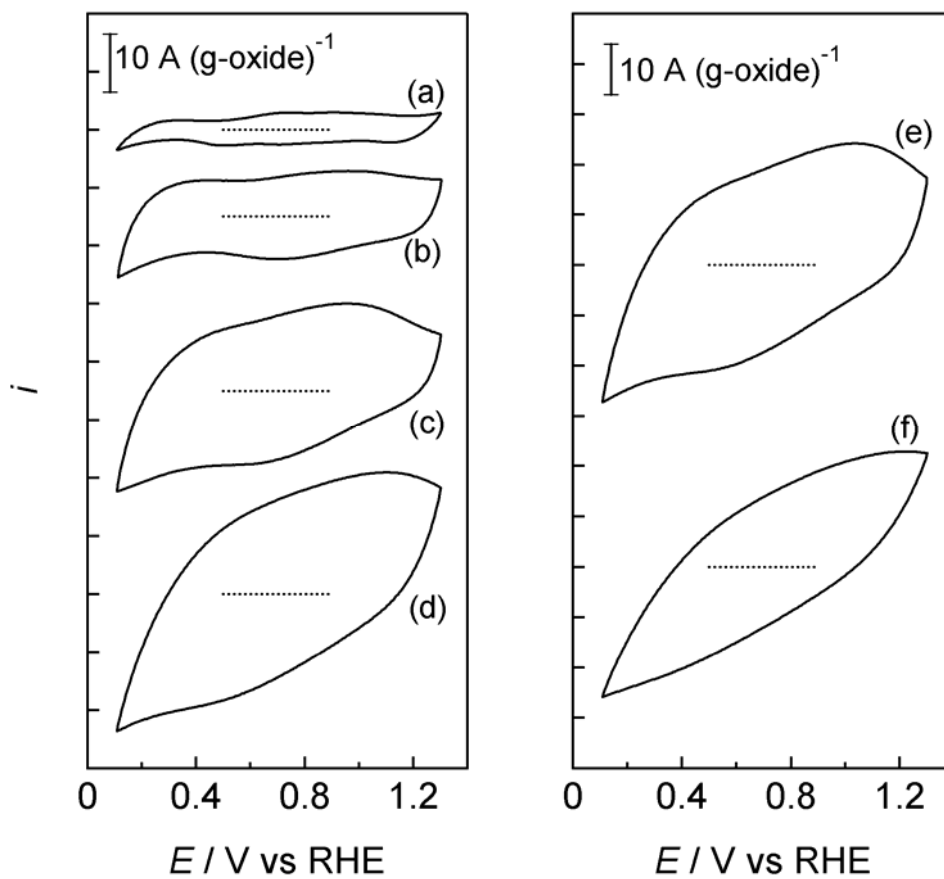


Fig.4. Steady-state cyclic voltammograms of (a)  $\text{RuO}_2$ , (b)  $\text{Ru}_{0.82}\text{V}_{0.18}\text{O}_2$ , (c)  $\text{Ru}_{0.63}\text{V}_{0.37}\text{O}_2$ , (d)  $\text{Ru}_{0.54}\text{V}_{0.46}\text{O}_2$ , (e)  $\text{Ru}_{0.41}\text{V}_{0.59}\text{O}_2$ , and (f)  $\text{Ru}_{0.35}\text{V}_{0.65}\text{O}_2$  thick films in 0.5 M  $\text{H}_2\text{SO}_4$  at a scan rate of  $50 \text{ mV s}^{-1}$ .

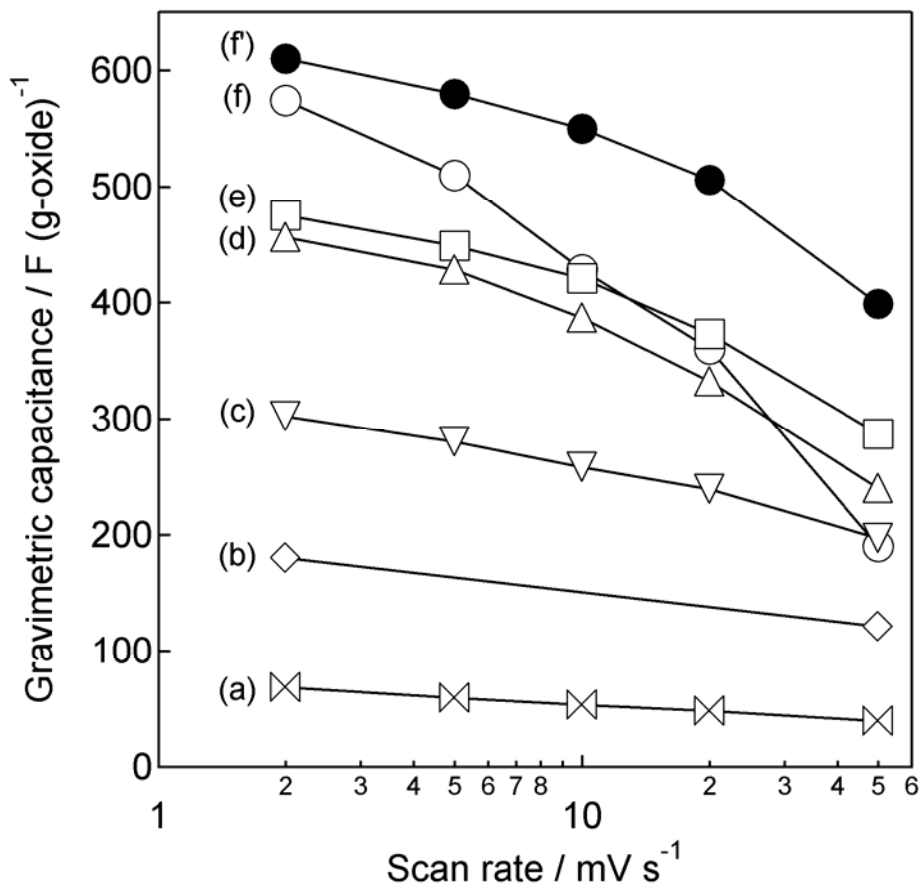


Fig.5. Scan-rate dependence of the gravimetric capacitance for (a) RuO<sub>2</sub>, (b) Ru<sub>0.82</sub>V<sub>0.18</sub>O<sub>2</sub>, (c) Ru<sub>0.63</sub>V<sub>0.37</sub>O<sub>2</sub>, (d) Ru<sub>0.54</sub>V<sub>0.46</sub>O<sub>2</sub>, (e) Ru<sub>0.41</sub>V<sub>0.59</sub>O<sub>2</sub>, (f) Ru<sub>0.35</sub>V<sub>0.65</sub>O<sub>2</sub> thick films. (f') Scan-rate dependence of the gravimetric capacitance of a Ru<sub>0.35</sub>V<sub>0.65</sub>O<sub>2</sub> thick film mixed with 20 mass% AB. The gravimetric capacitances were calculated from cyclic voltammograms between 0.1 and 1.3 V vs. RHE.

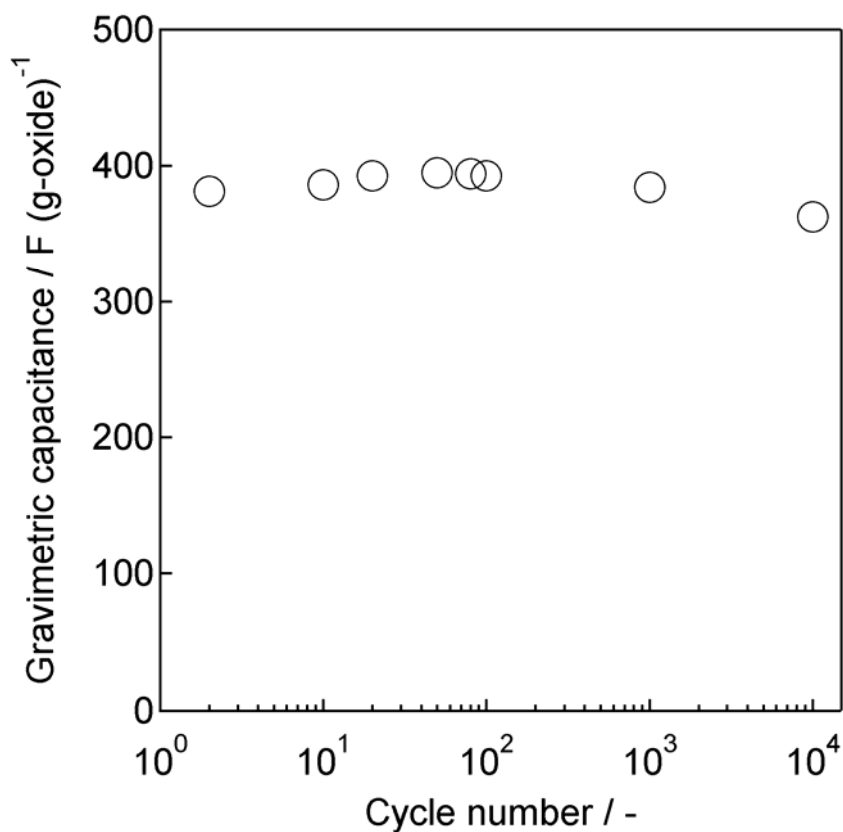


Fig. 6. Cyclability of  $\text{Ru}_{0.35}\text{V}_{0.65}\text{O}_2$  mixed with 20 mass% AB thick film at a scan rate of  $50 \text{ mV s}^{-1}$  in  $0.5 \text{ M H}_2\text{SO}_4$ . The gravimetric capacitances were calculated from cyclic voltammograms at a scan rate of  $50 \text{ mV s}^{-1}$  between  $0.1$  and  $1.3 \text{ V vs. RHE}$ .

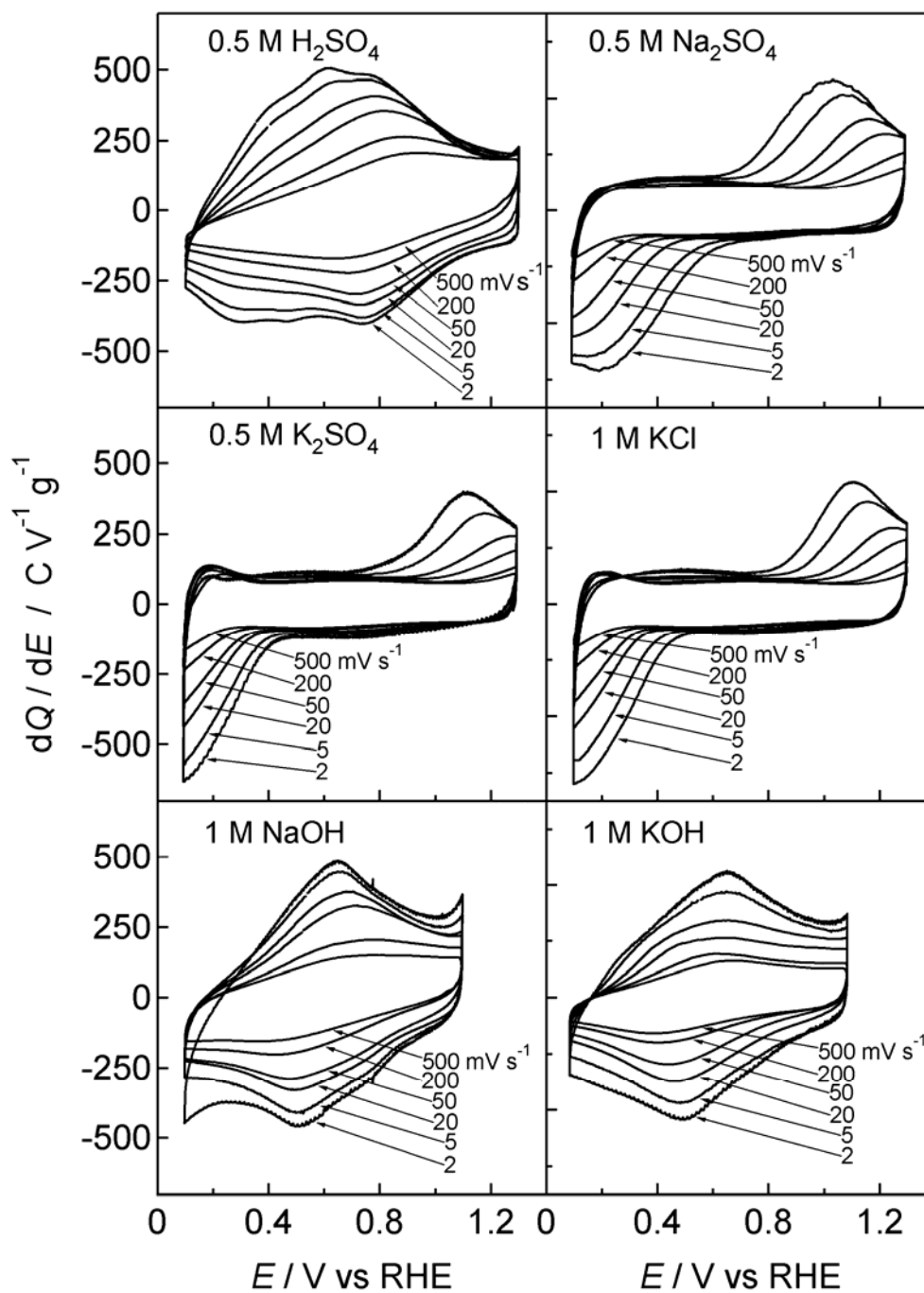


Fig. 7 Cyclic voltammograms showing the differential capacitance of  $\text{Ru}_{0.28}\text{V}_{0.72}\text{O}_2$  thin films in various electrolytes.